Sorption properties and reversibility of Ti(IV) and Nb(V)-fluoride doped-$Ca(BH_4)_2$-MgH_2 system

Christian Bonatto Minella, Sebastiano Garroni, Claudio Pistidda, Maria Dolors Baró, Oliver Gutfleisch, Thomas Klassen, Martin Dornheim

PII: S0925-8388(14)02681-4
DOI: http://dx.doi.org/10.1016/j.jallcom.2014.11.038
Reference: JALCOM 32587

To appear in: *Journal of Alloys and Compounds*

Received Date: 25 August 2014
Revised Date: 28 October 2014
Accepted Date: 5 November 2014

Please cite this article as: C.B. Minella, S. Garroni, C. Pistidda, M.D. Baró, O. Gutfleisch, T. Klassen, M. Dornheim, Sorption properties and reversibility of Ti(IV) and Nb(V)-fluoride doped-$Ca(BH_4)_2$-MgH_2 system, *Journal of Alloys and Compounds* (2014), doi: http://dx.doi.org/10.1016/j.jallcom.2014.11.038

Sorption properties and reversibility of Ti(IV) and Nb(V)-fluoride doped-$Ca(BH_4)_2$-MgH_2 system

Christian Bonatto Minella[1,2,#,*], Sebastiano Garroni[3], Claudio Pistidda[4], Maria Dolors Baró[5], Oliver Gutfleisch[6], Thomas Klassen[4], Martin Dornheim[4]

[1]Institute for Metallic Materials, IFW Dresden, Helmholtzstrasse 20, D-01069 Dresden, Germany

[2]Technische Universität Dresden, D-01062 Dresden, Germany

[3]Dipartimento di Chimica e Farmacia, Universitá di Sassari and INSTM, Via Vienna 2, I-07100 Sassari, Italy

[4]Institute of Materials Research, Materials Technology, Helmholtz-Zentrum Geesthacht, Zentrum für Material- und Küstenforschung GmbH, Max Planck Str. 1, D-21502 Geesthacht, Germany

[5]Departament de Física, Universitat Autònoma de Barcelona, E-08193 Bellaterra, Spain

[6]Materials Science, Technische Universität Darmstadt, Alarich-Weiss-Str. 16, 64287 Darmstadt, Germany

#Current address: Institute of Nanotechnology, Karlsruhe Institute of Technology (KIT), Hermann-von-Helmholtz-Platz 1, 76344 Eggenstein-Leopoldshafen, Germany

Corresponding author (*) = Christian Bonatto Minella

Mail: christian.minella@kit.edu

Telephone: +49 721 608-22680

Fax: +49 721 608-26368

Abstract

In the last decade, alkaline and alkaline earth metal tetrahydroborates have been the focuses of the research due to their high gravimetric and volumetric hydrogen densities. Among them, $Ca(BH_4)_2$ and the $Ca(BH_4)_2 + MgH_2$ reactive hydride composites (RHC), were calculated to have the ideal thermodynamic properties which fall within the optimal range for mobile applications.

In this study, the addition of NbF_5 or TiF_4 to the $Ca(BH_4)_2 + MgH_2$ reactive hydride composite system was attempted aiming to obtain a full reversible system with the simultaneous suppression of $CaB_{12}H_{12}$.

Structural characterization of the specimens was performed by means of *in-situ* Synchrotron Radiation Powder X-ray diffraction (SR-PXD) and $^{11}B\{^1H\}$ Solid State Magic Angle Spinning-Nuclear Magnetic Resonance (MAS-NMR). The evolution of the chemical state of the Nb- and Ti-based additives was monitored by X-ray Absorption Near Edge Structure (XANES).

The addition of NbF_5 or TiF_4 to the $Ca(BH_4)_2 + MgH_2$ system have not suppressed completely the formation of $CaB_{12}H_{12}$ and only a slight improvement concerning the reversible reaction was displayed just in the case of Nb-doped composite material.

Keywords

Hydrogen Storage, Transition Metal Fluorides, Tetrahydroborate, *In-situ* Synchrotron Radiation Powder X-ray diffraction (SR-PXD), X-ray Absorption Near Edge Structure (XANES), $^{11}B\{^1H\}$ Solid State Magic Angle Spinning-Nuclear Magnetic Resonance (MAS-NMR)

1. Introduction

The independence from a petroleum-based economy passes through the exploitation of hydrogen as a fuel. Nevertheless, its storage in a safe, efficient and convenient way still represents the main issue. Among other chemical fuels, hydrogen offers the highest energy density per unit of weight.[1] In addition, it does not pollute because when it is produced by renewable energy (*e.g.* solar), stored in a medium and burned in a fuel cell, only water vapor is produced as waste.[2]

In the last decade, alkaline and alkaline earth metal tetrahydroborates have been the focuses of the research due to their high gravimetric and volumetric hydrogen densities.[3] Among them, $Ca(BH_4)_2$ and the $Ca(BH_4)_2 + MgH_2$ reactive hydride composites (RHC) are considered one of the most interesting because calculations have demonstrated that they possess ideal thermodynamic properties which meet the requirements of the automotive technology.[4] $Ca(BH_4)_2 + MgH_2$ composite system, for instance, offers both a 10.5 wt. % theoretical hydrogen storage capacity and an estimated equilibrium temperature lower than 160 °C. [5] If MgB_2 forms upon desorption, the system offers better reaction enthalpy and faster re-hydrogenation kinetics. [5] However, experimental results reported in the literature do not match the predictions of the calculations. The sorption kinetics is, generally, sluggish and only partial reversibility was achieved so far. [6-10] In fact, besides CaH_2 and H_2, the decomposition of calcium borohydride leads to the formation of boron or several boron-based compounds such as CaB_6, CaB_2H_2, CaB_2H_6 and $CaB_{12}H_{12}$.[11-14] The competition among these decomposition products lies in the range of a few kJ mol^{-1} H_2. [13] Moreover, so far, no evidence for the formation of MgB_2 upon desorption is reported.

The reasons for the unsuccessful full reversibility in the $Ca(BH_4)_2$ and the $Ca(BH_4)_2 + MgH_2$ reactive hydride composite system are linked to both the slow boron mass transport and the phase segregation of chemically very stable phases (*e.g.* boron, $CaB_{12}H_{12}$).[15,16]

The addition of transition-metal chlorides and fluorides ($TiCl_3$, NbF_5 and TiF_4) demonstrated to be beneficial to avoid the formation of boron and drive the decomposition reaction to CaB_6 which was reported to be essential for the occurrence of the reversible reaction. [10, 17, 18] In fact, when transition-metal chlorides and fluorides are combined with a hydride phase and subjected to the mechanochemical processing, they transforms into more stable compounds (*e.g.* transition-metal based nanoparticles) which might act as heterogeneous nucleation sites.[17]

In this study, the addition of NbF_5 or TiF_4 to the $Ca(BH_4)_2$ + MgH_2 reactive hydride composite system was attempted aiming to obtain a full reversible system with the simultaneous suppression of $CaB_{12}H_{12}$. Structural characterization was performed by means of *in-situ* Synchrotron Radiation Powder X-ray diffraction (SR-PXD) and $^{11}B\{^1H\}$ Solid State Magic Angle Spinning-Nuclear Magnetic Resonance (MAS-NMR). The evolution of the Nb- and Ti-based phases was monitored by X-ray Absorption Near Edge Structure (XANES).

The addition of NbF_5 or TiF_4 to the $Ca(BH_4)_2$ + MgH_2 system was not efficient in suppressing completely the formation of $CaB_{12}H_{12}$ and only a slight improvement concerning the reversible reaction is displayed just in case of the Nb-doped composite sample.

2. Material and Methods

Pure $Ca(BH_4)_2$ powder was obtained from Sigma-Aldrich. MgH_2 was purchased by Goldschmidt (purity 95%). The MgH_2 powder was pre-milled for 5 hours in a stainless steel vial under 1 bar argon atmosphere using a Spex Mixer Mill (model 8000) with 10:1 as ball to powder ratio. One gram of powder mixture, composed by commercial $Ca(BH_4)_2$ and premilled MgH_2, was milled together for 5 hours using a Spex Mixer mill (model 8000). The milling was performed in a stainless steel vial under 1 bar of argon pressure with 10:1 as ball to powder ratio (3 spheres of 3.5 g each one and 1 g of powder). Both powder handling and milling were done in an MBraun argon glovebox with H_2O and O_2 levels below 10 ppm to prevent contamination.

The sorption and kinetics properties were evaluated using a Sievert apparatus (Hydro Quebec/HERA Hydrogen Storage System). The de-hydrogenation was investigated by heating from room temperature (25 °C) up to 400 °C with 5 °C min^{-1} as heating rate in static vacuum (0.02 bar the starting pressure value). Re-hydrogenation was performed on the de-hydrogenated products at 350 °C and 145 bar H_2 for 24 hours.

Differential Scanning Calorimetry was performed in a Netzsch STA 409 C in 50 ml min^{-1} argon flow. The samples were investigated in the 25-500 °C temperature range with 5 °C min^{-1} as heating rate.

In-situ Synchrotron Radiation Powder X-ray diffraction (SR-PXD) was carried out at the synchrotron MAX-lab, Lund (Sweden) at the beamline I711. The beamline is equipped with a MAR165 CCD detector. An especially designed cell for *in-situ* diffraction studies on solid/gas reactions was employed. The powder samples were charged in a sapphire single crystal tube.

Every operation was performed in an argon filled glovebox with H_2O and O_2 levels below 0.1 ppm. Under the sapphire tube a thermocouple is mounted in order to control the temperature. A gas supply system was connected to the cell which allows changing of the gas atmosphere. The X-ray exposure time was 30 s per powder diffraction pattern. The experiments were done heating the powder from room temperature up to 400 °C with a scanning heating rate of 5 K min^{-1}. The FIT2D software was used to remove diffraction sapphire spots from the 2D pictures acquired.
The abundance of phases was evaluated using the Rietveld method (using the MAUD software). [19]
XANES (X-ray Absorption Near Edge Structure) measurements were performed in transmission mode at the synchrotron Hasylab, DESY (Hamburg), at the beamline A1 and C respectively. Spectra were collected at the Ti and Nb K-edge (4966 and 18986 eV respectively) under vacuum at ambient temperature. The as milled and de-hydrogenated/re-hydrogenated materials were mixed with dried cellulose powder for dilution before experiments. Then, materials were pressed into pellet and placed between two Kapton foils on aluminum sample holders. All powder handling and sample preparation was entirely performed in an argon filled glovebox. Ti-foil, TiB_2, Ti_2O_3, TiO_2 (anatase), TiO, TiF_3 and TiF_4 samples were used as a reference for the measurements at the Ti K-edge. Nb-foil, NbO, NbF_5, NbB_2, Nb_2O_5 and $MgNb_2O_6$ samples were used as a reference for the measurements at the Nb K-edge. EXAFS data processing was carried out by the software ATHENA and ARTHEMIS [20] two interactive graphical utility based on the IFFEFIT [21] library of numerical and X-ray Absorption Spectroscopy (XAS) algorithms. All data are normalized and pre-edge background is subtracted.
Solid State Magic Angle Spinning - Nuclear Magnetic Resonance (MAS-NMR) spectra were obtained using a Bruker Avance 400 MHz spectrometer with a wide bore 9.4 T magnet and employing a boron-free Bruker 4 mm CPMAS probe. The spectral frequency was 128.33 MHz for the ^{11}B nucleus and the NMR shifts are reported in parts per million (ppm) externally referenced to BF_3Et_2O. The powder materials were packed into 4 mm ZrO_2 rotors in an argon-filled glovebox and were sealed with tight fitting Kel-F caps. The one-dimensional (1D) $^{11}B\{^1H\}$ and ^{11}B MAS-NMR spectra were acquired after a 2.7 μs single π/2 pulse (corresponding to a radiofield strength of 92.6 kHz) and with the application of a strong ^1H signal decoupling by using the two-pulse phase modulation (TPPM) scheme. The spectra were recorded at a MAS spinning rate of 12 kHz. Sample spinning was performed using dry nitrogen gas. The recovery

delay was set to 10 s. NMR spectra were acquired at 20 °C (controlled by a BRUKER BCU unit).

3. Results and Discussion

The SR-PXD patterns (at room temperature) for all the starting materials milled with additives are presented in Figure 1. The Bragg peaks of γ-$Ca(BH_4)_2$ (orthorhombic) [22], β-$Ca(BH_4)_2$ (tetragonal) [23], MgH_2 and CaF_2 are visible. The values of the relative abundance of phases are reported in Table 1.

The differential scanning calorimetry curves for the Nb- and Ti- doped composite materials are showed in Figure 2. The Figure displays one broad endothermic event shifted to lower temperatures (ca. 30 °C) with respect to the pure $Ca(BH_4)_2$ + MgH_2 composite (dotted curve). The three endothermic events showed by the pure composite are not clearly visible in the curves of the doped materials. Likely, the single broad signal, in case of the doped composite materials, includes more than one event. A low intensity endothermic signal at ca. 380 °C is visible for the TiF_4-doped material. Since with calorimetry only, it cannot be confirmed that these endothermic events correspond exclusively to hydrogen desorption reactions, the above mentioned materials were analyzed in the Sievert apparatus.

Figure 3 shows the kinetic curves of the first desorption reaction of the composite milled with the additives, obtained by thermovolumetric measurements. For comparison purposes, the desorption curve for pure ball milled $Ca(BH_4)_2$ + MgH_2 composite system is reported as well.

The Figure evidences that the addition of transition metal fluorides changes the desorption kinetics. Whereas in the ball milled $Ca(BH_4)_2$ + MgH_2 pure composite the hydrogen starts to be released around 350 °C, in the samples with additives the de-hydrogenation reaction begins already at 125 °C. Such a low temperature hydrogen desorption reaction was already observed for the $Ca(BH_4)_2$ system milled with transition metal fluorides additives [10].

While the pure ball milled $Ca(BH_4)_2$ + MgH_2 desorbs 6.4 wt. % hydrogen (in 3 hours) under the applied conditions, the samples with additives desorbs ca. 6.2 wt. % and ca. 5.8 wt. % H_2 respectively. The reason for the reduced hydrogen capacity delivered will be explained later.

In-situ SR-PXD was employed to obtain a comprehensive understanding of the sequence of reactions occurring during hydrogen desorption for the samples doped with NbF_5 and TiF_4.

The *in-situ* SR-PXD patterns over the temperature are reported in Figure 4 for the material milled with NbF_5 [24]. If not otherwise indicated, the desorption reaction was studied under static vacuum by heating from room temperature up to 400°C.

The XRD pattern at 30 °C evidences the reflections of CaF_2. CaF_2 originates from an the irreversible reaction between $Ca(BH_4)_2$ and NbF_5 during milling.[10,24] Its formations reduces the overall hydrogen capacity. The SR pattern at 217 °C shows that most of all the γ-phase has transformed into the β-phase. At 304 °C, the reflections of the β-$Ca(BH_4)_2$ decrease their intensity whereas $Ca_4Mg_3H_{14}$, $CaF_{2-x}H_x$, Mg and MgO phase appear. The absence of MgH_2 together with the reduced fraction of β-$Ca(BH_4)_2$ phase indicate that the hydrogen desorption step, at 304 °C, is approaching the end. The ternary Ca-F-H phase is formed as decomposition product by the reaction between CaH_2 and CaF_2.[10] The ternary $Ca_4Mg_3H_{14}$ phase decomposes in the 304-327 °C temperature range into CaH_2, Mg and H_2. Yet, the pattern at 304 °C displays the signal of the MgO phase. Albeit the samples were handled in inert atmosphere, formation of MgO could not be avoided. However, it seems that oxygen contaminations are already included in the starting $Ca(BH_4)_2$ material.[25] MgO reduces the amount of hydrogen measured by Sievert analysis (Figure 3). The final de-hydrogenated products, $CaF_{2-x}H_x$, Mg and MgO, are highlighted in the SR pattern at 400 °C. No trace of any boron-phase was detected by *in-situ* SR-PXD.

The *in-situ* SR-PXD patterns for the material milled with TiF_4 are reported in Figure 5.

CaF_2 is visible in this sample as well.[10] The SR pattern at 190 °C shows the phase transformation from γ- into the β-phase. At 304 °C, the reflections of the $Ca_3(^{11}BH_4)_3(^{11}BO_3)$ phase appear. [25] This phase is the responsible for the second hydrogen desorption step of $Ca(BH_4)_2$ and it was not observed in the case of the sample milled with NbF_5. The pattern at 343 °C displays the decomposition products. The two hydrogen desorption reactions occur in the 304-343 °C temperature range and when $Ca_4Mg_3H_{14}$ phase decomposes (pattern at 343 °C) respectively. At 343 °C, the reflections of $Ca_4Mg_3H_{14}$ decrease their intensity. In the 343-400 °C temperature range, $Ca_4Mg_3H_{14}$ decomposes into CaH_2, Mg and H_2. Furthermore, at 343 °C, beside $CaF_{2-x}H_x$, the signal of the MgO phase appears. The final de-hydrogenation products at 400 °C are $CaF_{2-x}H_x$, Mg, MgO and CaB_6. The Bragg peaks of the calcium hexaboride are broad indicating an amorphous-like or nano-size microstructure. [10] No trace of other boron-phases (*e.g.* $CaB_{12}H_{12}$) is detected by *in-situ* SR-PXD.

The re-hydrogenation reaction was attempted on the dehydrogenated products at 145 bar H_2 pressure and 350 °C for 24 hours. SR-PXD diffraction was carried out on the re-absorbed materials doped with NbF_5 and TiF_4 and the results are reported in Figure 6.

Figure 6 displays, for either patterns, the diffraction peaks of the α-$Ca(BH_4)_2$ phase. Hence, reversible formation was achieved. Nevertheless, the de-hydrogenated product $CaF_{2-x}H_x$ is also visible indicating that the reversibility is just partial. Compared to the pure system, no trace of CaH_2 can be detected in the SR-PXD patterns. [17] Instead, reflections of the $Ca_4Mg_3H_{14}$ show up. CaH_2 signals are absent because of the reaction with MgH_2 to form the ternary Ca-Mg-H phase. The re-hydrogenated material shows only the α- polymorph whereas the starting $Ca(BH_4)_2$ powder contained a mixture of the γ- and β- polymorph. The α- modification has an higher energetic stability compared to the other polymorphs. [26]

$^{11}B\{^1H\}$ MAS-NMR was undertaken aiming to detect amorphous or nanocrystalline boron-based compounds which cannot be revealed by diffraction techniques. The spectra are reported in Figure 7.

The NMR spectrum of the pure milled $Ca(BH_4)_2 + MgH_2$ composite shows two lines at -30 and -32 ppm corresponding to the γ (orthorhombic as the α-phase) and to the β-$Ca(BH_4)_2$ (tetragonal) phase respectively.[10] $CaB_{12}H_{12}$ provides a signal at -15.4 ppm.[16, 27] MgB_2 signal falls at ca. 100 ppm.[27, 28] The CaB_6 spectrum exhibits two lines, at +12 and +0.75 ppm, due to the two different boron sites in its structure.[29] The material after first desorption evidences three broad signals: +16, -15.6 and -30 ppm. The peaks at +16 and at -30 ppm are linked to the CaB_6 and to the residual β-$Ca(BH_4)_2$ respectively. The signal at -15.6 ppm belongs to $CaB_{12}H_{12}$.[8, 27]

The material after second hydrogen desorption show the same three peaks (at +16, -15.6 and -30 ppm) observed for the samples after first hydrogen desorption. The signals belong to CaB_6, $CaB_{12}H_{12}$ and residual β-$Ca(BH_4)_2$ respectively. XRD analysis evidenced that pure Mg and $CaF_{2-x}H_x$ are also present among the final products (Figure 4 and 5). MgO (traces) forms as well. Figure 7 (2nd Desorption) shows that only in case of the Ti-doped composite, the quantity of $CaB_{12}H_{12}$ formed is either reduced or its particles size become smaller over cycling. If a lower concentration of $CaB_{12}H_{12}$ is likely, a better reversibility respect to the pure composite system should be observed. Instead, a value of 3.2 wt. % of hydrogen (not shown here) is released for the Ti-doped system after second de-hydrogenation. As a matter of fact, this value attributes to the TiF_4 doped composite system a reversibility of 55 % which is exactly the same value

observed for the pure composite system. Hence, no improvement in terms of reversibility is found for the Ti-doped composite respect to the pure one. The Nb-doped system after second desorption (not shown here), instead, delivers 4 wt. % H_2. Therefore, a slight improvement of the reversibility (65 %) compared to the pure composite (55 %) is observed.

The Nb-phase formed during sorption reactions was investigated by XANES (X-ray Absorption Near Edge Structure). XANES curves, measured at the Nb K-edge (18986 eV), are represented in Figure 8. For comparison purposes, the spectrum of the material after ball milling and after first hydrogen desorption, are reported as well [24].

Figure 8 shows that a reaction between NbF_5 and the $Ca(BH_4)_2 + MgH_2$ composite has occurred during milling [24]. In addition, the Figure indicates that, after milling, the oxidation state of the Nb species reduces irreversibly. The curves corresponding to the milled and desorbed materials match that of NbB_2 (measured as a reference). Therefore, it can be concluded that Nb has reduced its oxidation state from (V) to (II). Just as a mere estimation it can be claimed that a Nb-B bond exists in the first coordination shell since the curves of the milled, desorbed and the NbB_2 materials are overlapping along the EXAFS (Extended X-ray Absorption Fine Structure) region (at higher energies respect to the Nb absorption K-edge). This assumption needs, nevertheless, to be confirmed by the Fourier Transform analysis of the EXAFS data.

The addition of TiF_4 to the $Ca(BH_4)_2 + MgH_2$ composite system does not exhibit any striking effect on the reversibility. However, for the understanding of the reaction mechanism it is necessary to know the nature of the Ti phase formed upon hydrogen sorption process.

XANES analysis at the Ti K-edge (4966 eV), including the curve for the ball milled and re-absorbed material, are reported in Figure 9.

The analysis of the curves, in the pre-edge region of the spectra, suggests that a reaction between the $Ca(BH_4)_2 + MgH_2$ composite and TiF_4 has occurred during milling [24]. In fact, the signal at 4971 eV for the TiF_4 curve is not visible anymore in the curve of the milled sample. SR-PXD has shown formation of CaF_2 after milling which is a evidence that a reaction has taken place in the vial (Figure 1 and 5). The curve of the milled sample, at the absorption edge, matches those of TiO_2 and Ti_2O_3. TiF_4 is not taken into account because it has reacted with $Ca(BH_4)_2$ to form CaF_2. Formation of Ti-oxides is plausible because of the oxygen contaminations contained within the starting $Ca(BH_4)_2$ material. [25] Nevertheless, within the rising edge region (at higher energies compared to the pre-edge region) the curve of the milled sample overlaps that of pure

TiO_2. This result is similar to what observed for the TiF_4 doped $Ca(BH_4)_2$ system. [10] However, Buslaev *et al.*[30] would exclude formation of TiO_2 as a product of the hydrolysis reaction of TiF_4. As a matter of fact, it can be concluded that for the milled sample, Ti has an oxidation state between IV (TiO_2) and III (Ti_2O_3).

The re-hydrogenated material shows further reduction in the oxidation state of Ti. Formation of TiB_2 seems to be promoted. Instead, within the rising edge region, the curve of the re-absorbed material falls between those of pure Ti_2O_3 and TiO_2. Combining these observations, it can be concluded that Ti might have evolved to a compound with an oxidation state between II (TiB_2) and III (Ti_2O_3) or a mixture of both different chemical states.[31]

4. Conclusions

A comprehensive investigation of the effect of TiF_4 and NbF_5 on the reversible hydrogenation reaction of the $Ca(BH_4)_2$ + MgH_2 composite system was carried out by means of several investigation tools.

Partial re-hydrogenation was achieved. XANES data evidenced the formation of transition metal boride nanoparticles either after milling or upon sorption reactions for the Ti- and Nb-based $Ca(BH_4)_2$ + MgH_2 doped composite systems. The full re-hydrogenation reaction is still hindered by the formation of $CaB_{12}H_{12}$ which is highly stable. The reaction leading to the $[B_{12}H_{12}]^{2-}$ is very favored and the transition metal borides nanoparticles are not able to both drive the desorption reaction to other boron-based compounds and to allow boron mass transport of very stable segregated phases.

As a matter of fact, on one hand, the addition of transition metal fluorides leads to the formation of transition metal boride nanoparticles as evidenced by XANES. On the other hand, side formation of CaF_2 is promoted which reduces the overall hydrogen content. Oxides-contamination in the starting material also limits irreversibly the re-hydrogenation reaction.

Moreover, it seems that transition metal boride nanoparticles are not able to overtake the extremely positive effect of Mg on the reversible formation of the $Ca(BH_4)_2 – MgH_2$ composite system as already reported in the literature. [32]

Acknowledgments

The authors are grateful to the Marie-Curie European Research Training Network (Contract MRTN- CT-2006-03 5366/COSY) and to the German Bundesministerium für Bildung und Forschung (Förderkennzeichen 03BV108C) for the financial support. C.B.M and O.G. thank the European Union (ERDF) and the Free State of Saxony (SAB Grant-Nr. 100112628). The I711 beamline staff, K. P. Pranzas and A. Schreyer are gratefully acknowledged. We are thankful to Pau Nolis and the Servei de Resonancia Magnetica Nuclear (RMN) at UAB for their technical assistance. E. Deprez is kindly acknowledged by C.B.M for useful discussion on XAS data. M.D.B. thanks partial financial support from an ICREA-Academia award.

Tables

Table 1

Phase	$Ca(BH_4)_2 + MgH_2 + \mathbf{NbF_5}$	$Ca(BH_4)_2 + MgH_2 + \mathbf{TiF_4}$
γ-$Ca(BH_4)_2$	40 wt. % (± 5 error)	41 wt. % (± 5 error)
β-$Ca(BH_4)_2$	45 wt. % (± 5 error)	46 wt. % (± 5 error)
MgH_2	9 wt. % (± 5 error)	9 wt. % (± 5 error)
CaF_2	6 wt. % (± 5 error)	4 wt. % (± 5 error)

Captions

Table 1. Phase abundances calculated by Rietveld method for the TiF_4- and NbF_5-doped $Ca(BH_4)_2 + MgH_2$ composite system.

Figure 1. XRD patterns after milling of the $Ca(BH_4)_2 + MgH_2$ composite milled with 0.05 mol of NbF_5 and TiF_4. γ-$Ca(BH_4)_2$ (γ); β-$Ca(BH_4)_2$ (β); MgH_2 (⊗); CaF_2 (◇).

Figure 2. DSC curves at 50 ml min^{-1} argon flow of ball milled $Ca(BH_4)_2 + MgH_2$ (dotted); $Ca(BH_4)_2 + MgH_2$ + 0.05 mol of NbF_5 (blue); $Ca(BH_4)_2 + MgH_2$ + 0.05 mol of TiF_4 (dark yellow).

Figure 3. Volumetric measurements showing the desorption curves over the temperature. Desorption curve of the pure $Ca(BH_4)_2 + MgH_2$ composite (black); $Ca(BH_4)_2 + MgH_2$ + 0.05 mol of NbF_5 (blue); $Ca(BH_4)_2 + MgH_2$ + 0.05 mol of TiF_4 (dark yellow).

Figure 4. SR-PXD patterns of $Ca(BH_4)_2 + MgH_2$ milled with 0.05 mol of NbF_5. The experiment was carried out by heating the sample in vacuum from RT up to 400 °C with 5 °C min^{-1} as heating rate. γ-$Ca(BH_4)_2$ (γ); β-$Ca(BH_4)_2$ (β); CaF_2 (◇); MgH_2 (⊗); $CaF_{2-x}H_x$ (∅); $Ca_4Mg_3H_{14}$ (∇); Mg (♣); MgO (◆).

Figure 5. SR-PXD patterns of $Ca(BH_4)_2 + MgH_2$ milled with 0.05 mol of TiF_4. The experiment was carried out by heating in vacuum from RT up to 400 °C with 5 °C min^{-1} as heating rate. γ-$Ca(BH_4)_2$ (γ); β-$Ca(BH_4)_2$ (β); CaF_2 (◇); $Ca_3(BH_4)_3(BO_3)$ (◖); $CaF_{2-x}H_x$ (∅); $Ca_4Mg_3H_{14}$ (∇); Mg (♣); MgO (◆); CaB_6 (⟐).

Figure 6. XRD of $Ca(BH_4)_2 + MgH_2$ doped with NbF_5 and TiF_4 after re-absorption reaction at 350 °C and 145 bar H_2 pressure for 24 hours. α-$Ca(BH_4)_2$ (α); $CaF_{2-x}H_x$ (∅); $Ca_4Mg_3H_{14}$ (∇); MgH_2 (⊗).

Figure 7. $^{11}B\{^1H\}$ MAS-NMR spectra at room temperature of pure $Ca(BH_4)_2$+ MgH_2 and milled with 0.05 mol of TiF_4 and NbF_5 after first hydrogen desorption (1st desorption) and after second

hydrogen desorption reaction (2^{nd} desorption). The NMR spectra of milled $Ca(BH_4)_2$+ MgH_2, MgB_2, CaB_6, $CaB_{12}H_{12}$ and boron are included. Side bands are indicated by ★, ▽, ∗, ✦, ⋆, ◇.

Figure 8. XANES data at the Nb K-edge for $Ca(BH_4)_2$ + MgH_2 + 0.05 mol of NbF_5 after ball milling and first hydrogen desorption.

Figure 9. XANES data at the Ti K-edge for the $Ca(BH_4)_2$ + MgH_2 + 0.05 mol of TiF_4 after ball milling and re-absorption process.

References

1. Dornheim M. Thermodynamics of Metal Hydrides: Tailoring Reaction Enthalpies of Hydrogen Storage Materials. Handbook of Hydrogen Storage; 2010.
2. Züttel A, Borgschulte A, Schlapbach L. Hydrogen as a Future Energy Carrier. Wiley-VCH; 2008.
3. Züttel A, Borgschulte A, Orimo S-I. Tetrahydroborates as new hydrogen storage materials. Scripta Mater 2007; 56: 823-8.
4. Miwa K, Aoki M, Noritake T, Ohba N, Nakamori Y, Towata S, Züttel A, Orimo S-I. Thermodynamical stability of calcium borohydride $Ca(BH_4)_2$. Phys Rev B 2006; 74: 155122.
5. Barkhordarian G, Klassen T, Dornheim M, Bormann R. Unexpected kinetic effect of MgB_2 in reactive hydride composites containing complex borohydrides. J Alloys Compd 2007; 440: L18 –L21.
6. Ronnebro E, Majzoub E H. Calcium borohydride for hydrogen storage: Catalysis and reversibility. J Phys Chem B 2007; 111: 12045-7.
7. Rongeat C, D'Anna V, Hagemann H, Borgschulte A, Züttel A, Schultz L, Gutfleisch O. Effect of additives on the synthesis and reversibility of $Ca(BH_4)_2$. J Alloys Compd 2010; 493: 281-7.
8. Bonatto Minella C, Garroni S, Olid D, Teixidor F, Pistidda C, Lindemann I, Gutfleisch O, Baró M D, Bormann R, Klassen T, Dornheim M. Experimental Evidence of

$Ca[B_{12}H_{12}]$ Formation During Decomposition of a $Ca(BH_4)_2$ + MgH_2 Based Reactive Hydride Composite. J Phys Chem C 2011; 115: 18010-4.

9. Kim Y, Hwang S-J, Shim J-H, Lee Y-S, Han H N, Cho Y W. Investigation of the Dehydrogenation Reaction Pathway of $Ca(BH_4)_2$ and Reversibility of Intermediate Phases. J Phys Chem C 2012; 116: 4330-4.
10. Bonatto Minella C, Garroni S, Pistidda C, Gosalawit-Utke R, Barkhordarian G, Rongeat C, Lindemann I, Gutfleisch O, Jensen T R, Cerenius Y, Christensen J, Baró M D, Bormann R, Klassen T, Dornheim M. Effect of Transition Metal Fluorides on the Sorption Properties and Reversible Formation of $Ca(BH_4)_2$. J Phys Chem C 2011; 115: 2497-504.
11. Ozolins V, Majzoub E H, Wolverton C. First-Principles Prediction of Thermodynamically Reversible Hydrogen Storage Reactions in the Li-Mg-Ca-B-H System. J Am Chem Soc 2009; 131: 230-7.
12. Wang L L, Graham D D, Robertson I M, Johnson D D. On the Reversibility of Hydrogen-Storage Reactions in $Ca(BH_4)_2$: Characterization via Experiment and Theory. J Phys Chem C 2009; 113: 20088-96.
13. Zhang Y S, Majzoub E, Ozolins V, Wolverton C. Theoretical prediction of different decomposition paths for $Ca(BH_4)_2$ and $Mg(BH_4)_2$. Phys Rev B 2010; 82: 174107.
14. Kim Y, Hwang S-J, Shim J-H, Lee Y-S, Han H N, Cho Y W. Investigation of the Dehydrogenation Reaction Pathway of $Ca(BH_4)_2$ and Reversibility of Intermediate Phases. J Phys Chem C 2012; 116: 4330-4.
15. Laubengayer A W, Hurd D T, Newkirk A E, Hoard J L. Boron I. Preparation and Properties of Pure Crystalline Boron. J Am Chem Soc 1943; 65: 1924-31.
16. Hermanek S. Boron-11 NMR spectra of boranes, main-group heteroboranes, and substituted derivatives. Factors influencing chemical shifts of skeletal atoms. Chem Rev 1992; 92: 325-62.
17. Bonatto Minella C, Pellicer E, Rossinyol E, Karimi F, Pistidda C, Garroni S, Milanese C, Nolis P, Baró M D, Gutfleisch O, Pranzas K P, Schreyer A, Klassen T, Bormann R, Dornheim M. Chemical State, Distribution, and Role of Ti- and Nb-Based Additives on the $Ca(BH_4)_2$ System. J Phys Chem C 2013; 117: 4394–403.

18. Kim J H, Jin S A, Shim J H, Cho Y W. Reversible hydrogen storage in calcium borohydride $Ca(BH_4)_2$. Scripta Mater 2008; 58: 481-3.
19. Lutterotti L, Matthies S, Wenk H R, Schultz A S, Richardson J W. Combined texture and structure analysis of deformed limestone from time-of-flight neutron diffraction spectra. J Appl Phys 1997; 81: 594-600.
20. Ravel B, Newville M. ATHENA, ARTEMIS, HEPHAESTUS: data analysis for X-ray absorption spectroscopy using IFEFFIT. J Synchrotron Radiat 2005; 12: 537-41.
21. Newville M. IFEFFIT : interactive XAFS analysis and FEFF fitting. J Synchrotron Radiat 2001; 8: 322-4.
22. Buchter F, Lodziana Z, Remhof A, Friedrichs O, Borgschulte A, Mauron P, Züttel A, Sheptyakov D, Palatinus L, Chlopek K, Fichtner M, Barkhordarian G, Bormann R, Hauback B C. Structure of the Orthorhombic gamma-Phase and Phase Transitions of $Ca(BD_4)_2$. J Phys Chem C 2009; 113: 17223-30.
23. Filinchuk Y, Ronnebro E, Chandra D. Crystal structures and phase transformations in $Ca(BH_4)_2$. Acta Mater 2009; 57: 732-8.
24. Bonatto Minella C, Effect of transition metal fluorides on the sorption properties of the $Ca(BH_4)_2$ and $Ca(BH_4)_2 + MgH_2$ composite system, PhD Thesis, Universitätsbibliothek der TU Hamburg-Harburg.
25. Riktor M D, Filinchuk Y, Vajeeston P, Bardaji E G, Fichtner M, Fjellvag H, Sorby M H, Hauback B C. The crystal structure of the first borohydride borate, $Ca_3(BD_4)_3(BO_3)$. J Mater Chem 2011; 21: 7188-93.
26. Borgschulte A, Gremaud R, Züttel A, Martelli P, Remhof A, Ramirez-Cuesta A J, Refson K, Bardaji E G, Lohstroh W, Fichtner M, Hagemann H, Ernst M. Experimental evidence of librational vibrations determining the stability of calcium borohydride. Phys Rev B 2011, 83, 024102.
27. Hwang S-J, Bowman R C Jr, Reiter J W, Rijssenbeek J, Soloveichik G L, Zhao J-C, Kabbour H, Ahn C C. NMR confirmation for formation of $B_{12}H_{12}^{2-}$ complexes during hydrogen desorption from metal borohydrides. J Phys Chem C 2008; 112: 3164 –9.
28. Pistidda C, Garroni S, Dolci F, Gil Bardaji E, Khandelwal A, Nolis P, Dornheim M, Gosalawit R, Jensen T R, Cerenius Y, Suriñach S, Baró M D, Lohstroh W, Fichtner M.

Synthesis of amorphous $Mg(BH_4)_2$ from MgB_2 and H_2 at room temperature. J Alloys Compd 2010; 508: 212–5.

29. Mean B J, Lee K H, Kang K H, Lee M, Rhee J S, Cho B K. B-11 NMR study of calcium-hexaborides. Phys B 2005; 359-361: 1204–6.
30. Buslaev Y A, Dyer D S, Ragsdale R O. Hydrolysis of titanium tetrafluoride. Inorg Chem 1967; 6: 2208-12.
31. Deprez, E, Muñoz-Marquez M A, Roldan M A, Prestipino C, Palomares F J, Bonatto Minella C, Bösenberg U, Dornheim M, Bormann R, Fernandez A. Oxidation State and Local Structure of Ti-Based Additives in the Reactive Hydride Composite $2LiBH_4$ + MgH_2. J Phys Chem C 2010; 114: 3309-17.
32. Bonatto Minella C, Pistidda C, Garroni S, Nolis P, Baró M D, Gutfleisch O, Klassen T, Bormann R, Dornheim M. $Ca(BH_4)_2$ + MgH_2: Desorption Reaction and Role of Mg on Its Reversibility. J Phys Chem C 2013; 117: 3846–52.

Figures

Figure 1

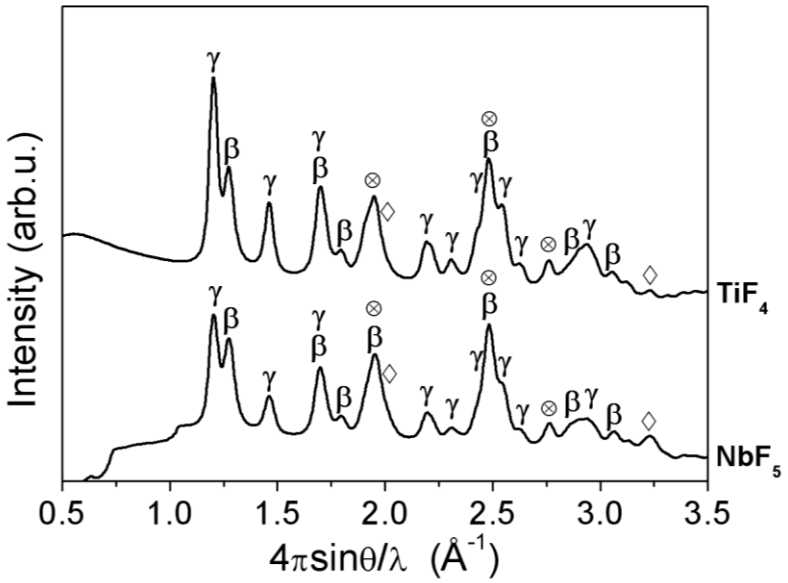

Figure 2

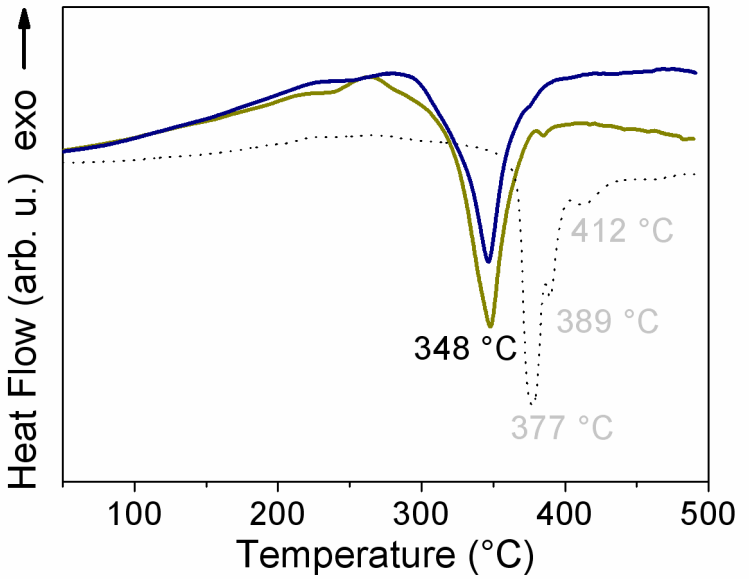

Figure 3

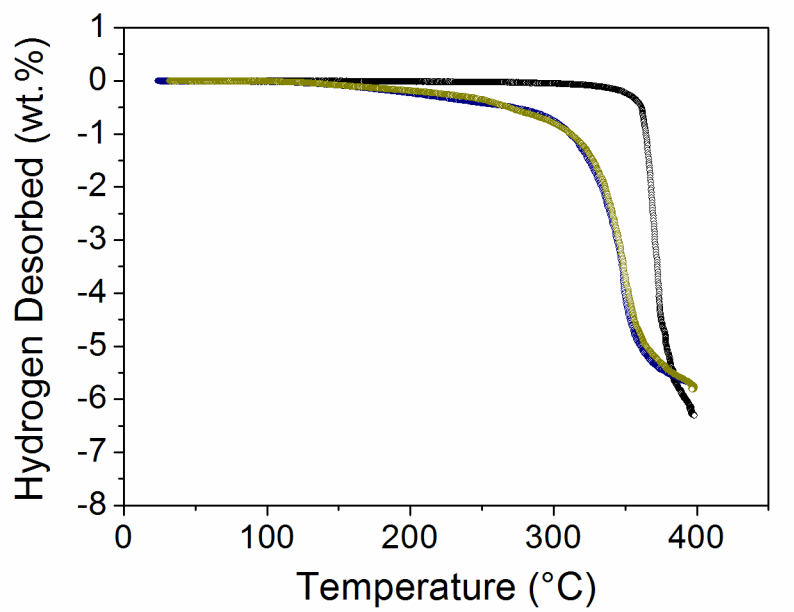

Figure 4

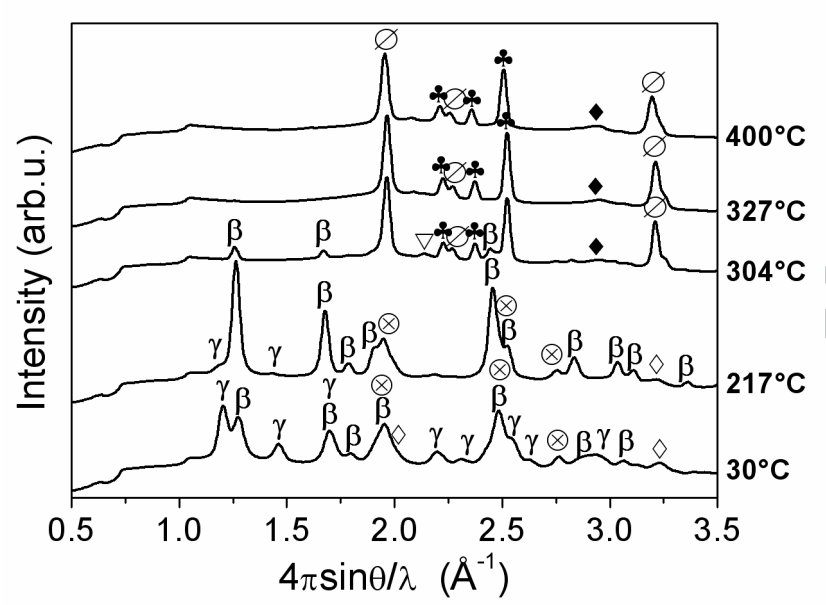

Figure 5

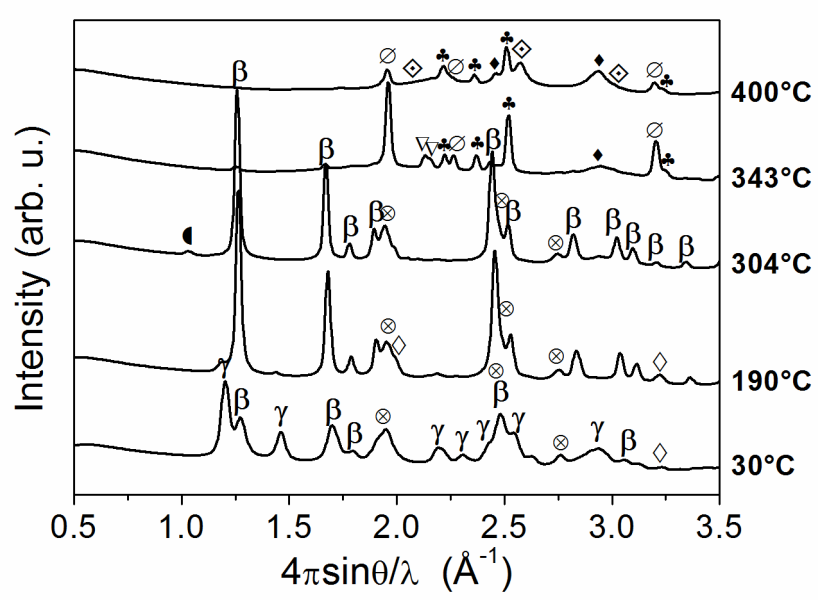

Figure 6

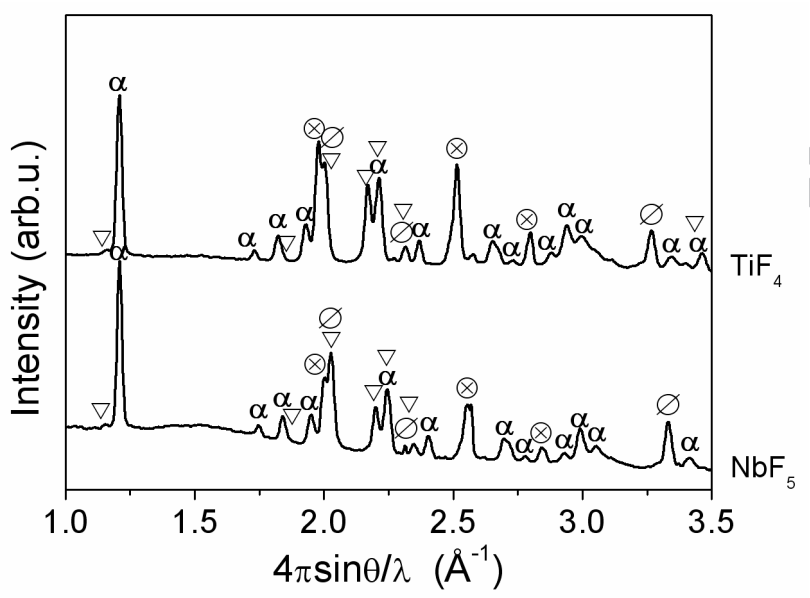

Figure 7

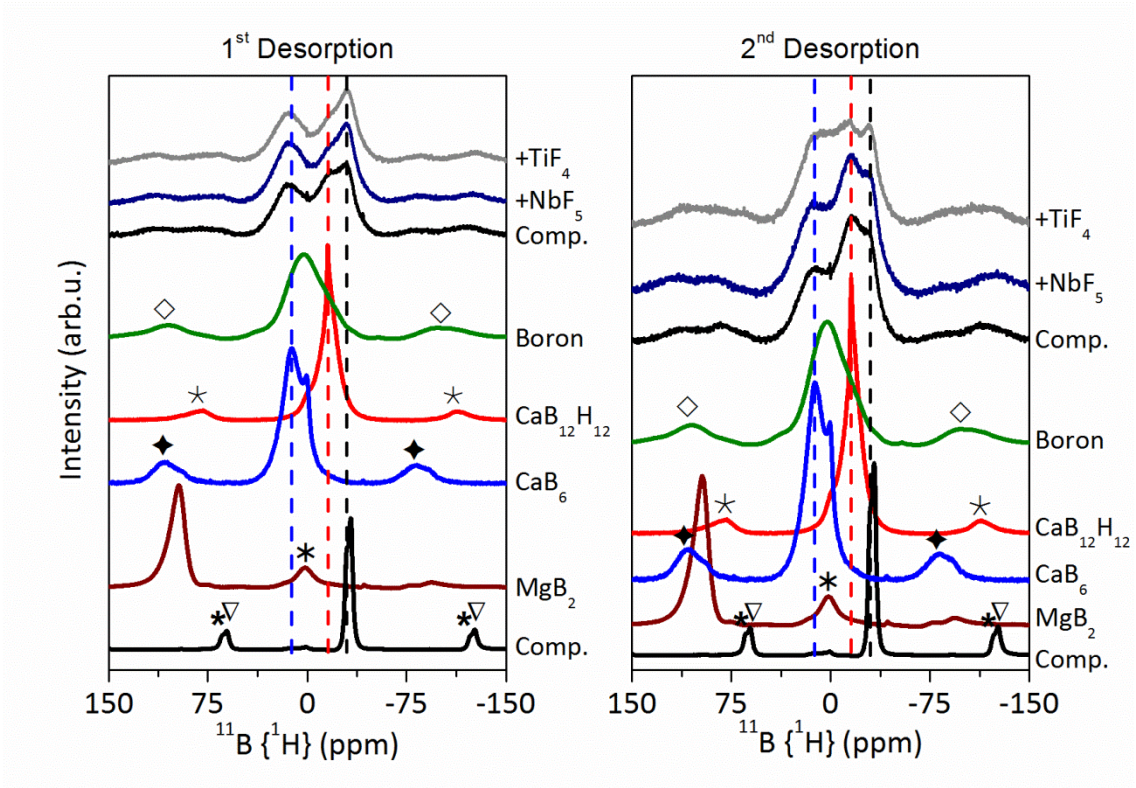

Figure 8

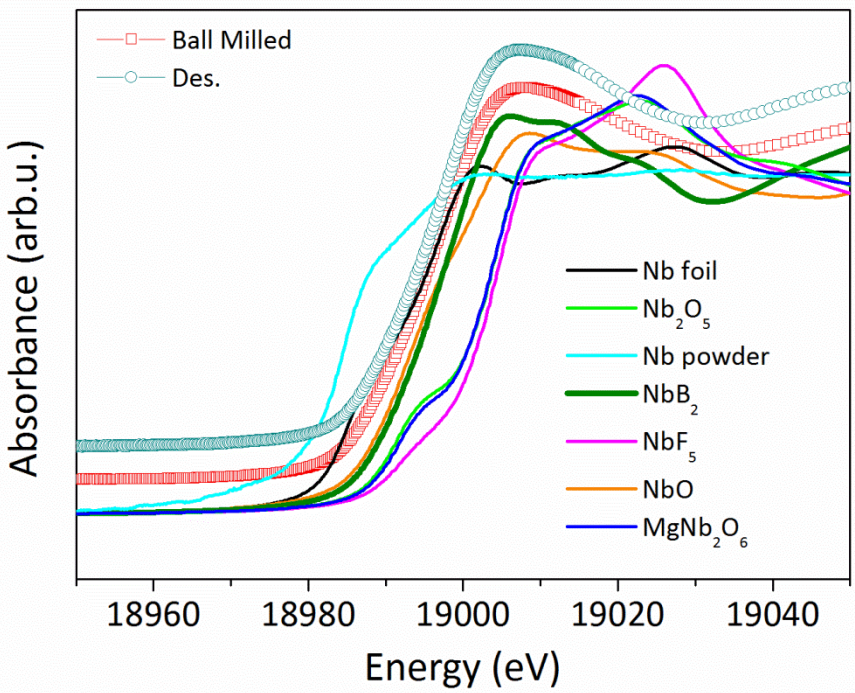

Figure 9

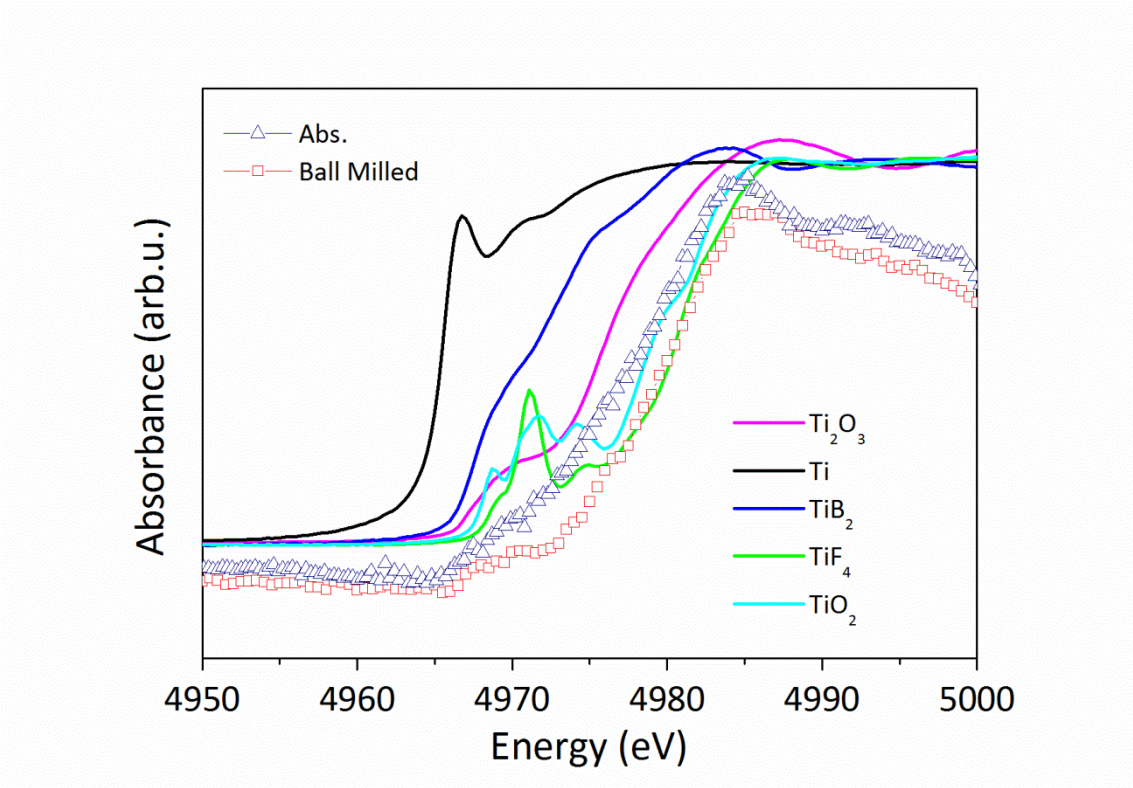

Highlights:

- Lower hydrogen desorption reaction evidenced by the addition of transition metal fluorides additives with respect to the pure composite system.
- Kinetic improvement concerning re-hydrogenation reaction showed by the addition of NbF_5.
- Full characterization of the de-hydrogenation reaction pathway by means of both SR-PXD and $^{11}B\{^1H\}$ MAS-NMR.
- Study of the evolution of the chemical state of the additives upon both milling and sorption reactions.